Measurement of the 77Se(n,γ) cross section up to 200 keV at the n_TOF facility at CERN

(n_TOF Collaboration) Sosnin, N. V.; Lederer-Woods, C.; Krtička, M.; Garg, R.; Dietz, M.; Bacak, M.; Barbagallo, M.; Battino, U.; Cristallo, S.; Damone, L. A.; ...

Source / Izvornik: **Physical Review C, 2023, 107**

Journal article, Published version
Rad u časopisu, Objavljena verzija rada (izdavačev PDF)

https://doi.org/10.1103/PhysRevC.107.065805

Permanent link / Trajna poveznica: https://urn.nsk.hr/urn:nbn:hr:217:198605

Measurement of the ^{77}Se(n, γ) cross section up to 200 keV at the n_TOF facility at CERN

N. V. Sosnin,[1,*] C. Lederer-Woods,[1] M. Krtička,[2] R. Garg,[1,3,4] M. Dietz,[1,5] M. Bacak,[6,7,8] M. Barbagallo,[6,9] U. Battino,[10] S. Cristallo,[11,12] L. A. Damone,[9,13] M. Diakaki,[14,6] S. Heinitz,[15] D. Macina,[6] M. Mastromarco,[6] F. Mingrone,[6] A. St. J. Murphy,[1] G. Tagliente,[9] S. Valenta,[2] D. Vescovi,[16] O. Aberle,[6] V. Alcayne,[17] S. Amaducci,[18,19] J. Andrzejewski,[20] L. Audouin,[21] V. Bécares,[17] V. Babiano-Suarez,[22] F. Bečvář,[2] G. Bellia,[18,19] E. Berthoumieux,[8] J. Billowes,[23] D. Bosnar,[24] A. Brown,[25] M. Busso,[12,26] M. Caamaño,[27] L. Caballero,[22] F. Calviño,[28] M. Calviani,[6] D. Cano-Ott,[17] A. Casanovas,[28] F. Cerutti,[6] Y. H. Chen,[21] E. Chiaveri,[6,23,29] N. Colonna,[9] G. Cortés,[28] M. A. Cortés-Giraldo,[29] L. Cosentino,[18] C. Domingo-Pardo,[22] R. Dressler,[15] E. Dupont,[8] I. Durán,[27] Z. Eleme,[30] B. Fernández-Domínguez,[27] A. Ferrari,[6] P. Finocchiaro,[18] K. Göbel,[31] A. Gawlik-Ramięga,[20] S. Gilardoni,[6] T. Glodariu,[32,†] I. F. Gonçalves,[33] E. González-Romero,[17] C. Guerrero,[29] F. Gunsing,[8] H. Harada,[34] J. Heyse,[35] D. G. Jenkins,[25] E. Jericha,[7] F. Käppeler,[36,†] Y. Kadi,[6] A. Kimura,[34] N. Kivel,[15] M. Kokkoris,[14] D. Kurtulgil,[31] I. Ladarescu,[22] H. Leeb,[7] J. Lerendegui-Marco,[29] S. Lo Meo,[37,38] S. J. Lonsdale,[1] A. Manna,[38,39] T. Martínez,[17] A. Masi,[6] C. Massimi,[38,39] P. Mastinu,[40] F. Matteucci,[41,42] E. A. Maugeri,[15] A. Mazzone,[9,43] E. Mendoza,[17] A. Mengoni,[37] V. Michalopoulou,[14] P. M. Milazzo,[41] A. Musumarra,[44,19] A. Negret,[32] R. Nolte,[5] F. Ogállar,[45] A. Oprea,[32] N. Patronis,[30] A. Pavlik,[46] J. Perkowski,[20] L. Piersanti,[9,12,47] I. Porras,[45] J. Praena,[45] J. M. Quesada,[29] D. Radeck,[5] D. Ramos-Doval,[21] T. Rauscher,[48,49] R. Reifarth,[31] D. Rochman,[15] C. Rubbia,[6] M. Sabaté-Gilarte,[6,29] A. Saxena,[50] P. Schillebeeckx,[35] D. Schumann,[15] A. G. Smith,[23] A. Stamatopoulos,[14] J. L. Tain,[22] T. Talip,[15] A. Tarifeño-Saldivia,[28] L. Tassan-Got,[6,14,21] P. Torres-Sánchez,[45] A. Tsinganis,[6] J. Ulrich,[15] S. Urlass,[6,51] G. Vannini,[38,39] V. Variale,[9] P. Vaz,[33] A. Ventura,[38] V. Vlachoudis,[6] R. Vlastou,[14] A. Wallner,[52] P. J. Woods,[1] T. Wright,[23] and P. Žugec[24] (n_TOF Collaboration)[‡]

[1]*School of Physics and Astronomy, University of Edinburgh, Edinburgh, United Kingdom*
[2]*Charles University, Prague, Czech Republic*
[3]*Facility for Rare Isotope Beams, Michigan State University, East Lansing, Michigan 48824, USA*
[4]*Department of Physics and Astronomy, Michigan State University, East Lansing, Michigan 48824, USA*
[5]*Physikalisch-Technische Bundesanstalt (PTB), Bundesallee 100, 38116 Braunschweig, Germany*
[6]*European Organization for Nuclear Research (CERN), Geneva, Switzerland*
[7]*Atominstitut, Stadionallee 2, TU Wien, 1020 Wien, Austria*
[8]*CEA Irfu, Université Paris-Saclay, F-91191 Gif-sur-Yvette, France*
[9]*Istituto Nazionale di Fisica Nucleare, Sezione di Bari, Bari, Italy*
[10]*E.A. Milne Centre for Astrophysics, Department of Physics and Mathematics, University of Hull, Hull, United Kingdom*
[11]*Istituto Nazionale di Astrofisica - Osservatorio Astronomico d'Abruzzo, Teramo, Italy*
[12]*Istituto Nazionale di Fisica Nucleare, Sezione di Perugia, Perugia, Italy*
[13]*Dipartimento Interateneo di Fisica, Università degli Studi di Bari, Bari, Italy*
[14]*National Technical University of Athens, Athens, Greece*
[15]*Paul Scherrer Institut (PSI), Villigen, Switzerland*
[16]*Goethe University Frankfurt, Max-von-Laue-Strasse 1, Frankfurt am Main D-60438, Germany*
[17]*Centro de Investigaciones Energéticas Medioambientales y Tecnológicas (CIEMAT), Madrid, Spain*
[18]*INFN Laboratori Nazionali del Sud, Catania, Italy*
[19]*Department of Physics and Astronomy, University of Catania, Catania, Italy*
[20]*University of Lodz, Lodz, Poland*
[21]*Institut de Physique Nucléaire, CNRS-IN2P3, Université Paris-Sud, Université Paris-Saclay, F-91406 Orsay Cedex, France*
[22]*Instituto de Física Corpuscular, CSIC - Universidad de Valencia, Valencia, Spain*
[23]*University of Manchester, Manchester, United Kingdom*
[24]*Department of Physics, Faculty of Science, University of Zagreb, Zagreb, Croatia*
[25]*University of York, York, United Kingdom*
[26]*Dipartimento di Fisica e Geologia, Università di Perugia, Perugia, Italy*
[27]*University of Santiago de Compostela, Santiago de Compostela, Spain*
[28]*Universitat Politècnica de Catalunya, Barcelona, Spain*
[29]*Universidad de Sevilla, Seville, Spain*

[*]Corresponding author: nsosnin@ed.ac.uk
[†]Deceased.
[‡]www.cern.ch/ntof.

[30]*University of Ioannina, Ioannina, Greece*
[31]*Goethe University Frankfurt, Frankfurt, Germany*
[32]*Horia Hulubei National Institute of Physics and Nuclear Engineering, Bucharest-Magurele, Romania*
[33]*Instituto Superior Técnico, Lisbon, Portugal*
[34]*Japan Atomic Energy Agency (JAEA), Tokai-Mura, Japan*
[35]*Joint Research Centre (JRC), European Commission, Geel, Belgium*
[36]*Karlsruhe Institute of Technology, Campus North, IKP, 76021 Karlsruhe, Germany*
[37]*Agenzia Nazionale per le Nuove Tecnologie (ENEA), Rome, Italy*
[38]*Istituto Nazionale di Fisica Nucleare, Sezione di Bologna, Bologna, Italy*
[39]*Dipartimento di Fisica e Astronomia, Università di Bologna, Bologna, Italy*
[40]*INFN Laboratori Nazionali di Legnaro, Legnaro, Italy*
[41]*Istituto Nazionale di Fisica Nucleare, Sezione di Trieste, Trieste, Italy*
[42]*Department of Physics, University of Trieste, Trieste, Italy*
[43]*Consiglio Nazionale delle Ricerche, Bari, Italy*
[44]*Istituto Nazionale di Fisica Nucleare, Sezione di Catania, Catania, Italy*
[45]*University of Granada, Granada, Spain*
[46]*University of Vienna, Faculty of Physics, Vienna, Austria*
[47]*Istituto Nazionale di Astrofisica - Osservatorio Astronomico di Teramo, Teramo, Italy*
[48]*Department of Physics, University of Basel, Basel, Switzerland*
[49]*Centre for Astrophysics Research, University of Hertfordshire, Hatfield, United Kingdom*
[50]*Bhabha Atomic Research Centre (BARC), Mumbai, India*
[51]*Helmholtz-Zentrum Dresden-Rossendorf, Dresden, Germany*
[52]*Australian National University, Canberra, Australia*

(Received 20 February 2023; revised 17 May 2023; accepted 23 May 2023; published 12 June 2023)

The ^{77}Se(n,γ) reaction is of importance for ^{77}Se abundance during the slow neutron capture process in massive stars. We have performed a new measurement of the ^{77}Se radiative neutron capture cross section at the Neutron Time-of-Flight facility at CERN. Resonance capture kernels were derived up to 51 keV and cross sections up to 200 keV. Maxwellian-averaged cross sections were calculated for stellar temperatures between $kT = 5$ keV and $kT = 100$ keV, with uncertainties between 4.2% and 5.7%. Our results lead to substantial decreases of 14% and 19% in ^{77}Se abundances produced through the slow neutron capture process in selected stellar models of $15M_{\odot}$ and $2M_{\odot}$, respectively, compared to using previous recommendation of the cross section.

DOI: 10.1103/PhysRevC.107.065805

I. MOTIVATION

The slow neutron capture process (*s* process) is responsible for about half of the elemental abundances between Fe and Bi in our solar system. The *s* process proceeds by a series of neutron captures on an iron seed distribution, with neutron capture being slower than β decays, resulting in a reaction flow that closely follows the valley of stability. A key nuclear physics quantity impacting on abundances produced in the *s* process is the neutron capture cross section averaged over the Maxwellian velocity distribution present in the stars, called Maxwellian averaged cross section (MACS). The weak component of the *s* process occurs in massive stars during He core and C shell burning phases at neutron densities of around 10^8 cm^{-3} [1]. This stellar site primarily contributes to the production of elements between Fe and Sr, which are ejected into the interstellar medium during the later core collapse supernova explosion. A recent study [2] found that present uncertainties in the ^{77}Se(n,γ) rate have the largest impact on ^{77}Se abundances predicted to be produced in the *s* process in massive stars compared to any other neutron capture or β-decay rate.

Existing experimental data on the ^{77}Se(n,γ) cross section at the relevant stellar energies are scarce. In massive stars, the *s* process takes place at stellar temperatures between 0.35 and 1 GK, which corresponds to $kT \approx 30$ and 90 keV, respectively, hence neutron capture cross sections are required to be known up to a few hundred keV energy. There is only one previous measurement of the neutron capture cross section at neutron energies E_n above 10 keV by Kamada *et al.* [3,4], who determined cross sections from 15 to 100 keV and at ≈510 keV in five neutron energy intervals (see Sec. III C). Measurements of ^{77}Se $+n$ reactions at lower neutron energy, including determination of some neutron resonance parameters, are published in [5–10]. Of these, Refs. [6–8] provide information on spin and partial radiative and neutron widths Γ_γ and Γ_n for a few observed resonances for $E_n < 4$ keV. These experimental resonance parameters form the basis of the evaluation by Mughabghab [11] and the latest ENDF/B-VIII.0 library [12].

Since MACS at stellar temperatures is given by cross section at neutron energies from keV to hundreds of keV, a new measurement of the ^{77}Se(n,γ) cross section was performed

TABLE I. Properties of the samples used in the experiment.

Sample	Chemical form	Mass (g)	Diameter (mm)	Sample composition (%)
^{77}Se	metal	0.9916	20	^{77}Se(99.66); ^{74}Se(0.02); ^{76}Se(0.14); ^{78}Se(0.09) ^{80}Se(0.05); ^{82}Se(0.04)
^{197}Au	metal	0.6441	20	^{197}Au (100)
C-nat	graphite	2.65	20	^{12}C (98.93); ^{13}C (1.07)

at the Neutron Time-of-Flight (n_TOF) Facility at CERN [13] making use of the facility's excellent energy resolution in the relevant neutron energy range. The details of the experiment are presented in Sec. II, data analysis and the results are described in Sec. III, the calculation of Maxwellian averaged cross sections and astrophysical implications are discussed in Sec. IV, and a summary is provided in Sec. V.

II. MEASUREMENT

The measurement presented in this work was conducted at the Neutron Time-of-Flight facility (n_TOF) at CERN. At n_TOF, neutrons are produced by spallation reactions of a 20 GeV/c proton beam from the Proton Synchrotron (PS) accelerator impinging on a massive lead target. The proton beam is pulsed with a frequency of 0.8 Hz and an rms time width of 7 ns. Water and borated water layers around the spallation target act as moderator and coolant, resulting in a neutron spectrum ranging from thermal neutron energies to ≈1 GeV. More details about the facility can be found in Ref. [14]. The n_TOF facility operates two experimental areas: one at a distance of 185 m from the spallation target (EAR-1), and one at 20 m (EAR-2). The ^{77}Se(n,γ) experiment took place at EAR-1, taking advantage of the excellent neutron energy resolution available (0.11% at 10 keV neutron energy [14]).

The ^{77}Se sample consisted of 1 g of 99.66% enriched Se metal powder which was pressed into a cylindrical shape of 2 cm diameter and 0.7 mm thickness. The sample was glued on a thin Mylar backing foil fixed onto an aluminum ring. In addition, a ^{197}Au sample was used in the experiment to normalize the data, and an empty sample holder and natural carbon sample were used to estimate the background. The dimensions and composition of all samples used in the experiment are listed in Table I. The prompt γ radiation emitted after neutron capture was detected with a set of four liquid scintillation detectors filled with deuterated benzene (C_6D_6), which were optimized to achieve an extremely low sensitivity to scattered neutrons [15]. Data were recorded by means of 14-bit digitizers operated at a sampling rate of 1 GHz. The data acquisition is triggered just before the proton beam hits the spallation target, and signal waveforms are written to disk for 100 ms after the trigger, corresponding to a minimum neutron energy of ≈0.02 eV. Signal arrival times and amplitudes are then extracted offline by applying a dedicated pulse-shape algorithm [16].

III. DATA ANALYSIS AND RESULTS

A. Experimental capture yield

The neutron flight path length was determined as 183.95 ± 0.04 m using known low-energy resonances in the ^{197}Au $+n$ reaction [12]. Following conversion of the time-of-flight data to neutron energy, counting spectra can be converted to capture yield $Y(E_n)$ using the expression

$$Y(E_n) = f(E_n)\frac{C(E_n) - B(E_n)}{\epsilon(E_n)\Phi(E_n)}. \quad (1)$$

Here, C are measured counts at a given neutron energy E_n, B are background counts, ϵ is detection efficiency, Φ is the neutron fluence, and f is normalization, which accounts for the sample not fully covering the neutron beam as well as inaccuracies in detector response simulations (discussed in Sec. III A 3).

1. Detection efficiency

The detection efficiency of a C_6D_6 scintillator depends on the γ-ray energy, hence the efficiency of detecting a neutron capture event depends on the deexcitation pattern of the compound nucleus. To compensate for its variation from different resonances, we used the total energy detection principle in conjunction with the pulse height weighting technique (PHWT) [17]. It is based on applying a pulse height dependent weight to each signal, resulting in a detection efficiency that is proportional to the excitation energy of the compound nucleus. The weighting function was calculated using simulations of the detector response to monoenergetic γ rays ranging from 100 keV to 10 MeV using GEANT4 Monte Carlo code [18], including a detailed geometry of the experimental setup. The analysis threshold for deposited energy $E_D > 200$ keV was adopted. The impact of low-energy transitions and electron conversion on the weighting function were taken into account by simulating neutron capture cascades for the ^{77}Se and Au samples with the code DICEBOX [19]. We estimate that the PHWT, including threshold corrections, introduces a 3% uncertainty to the capture yield.

2. Background subtraction

The background was measured by recording spectra without neutron beam (ambient background), and spectra with beam on an empty sample holder. The contribution of these background components relative to the sample spectrum is shown in Fig 1.

In addition, background may be caused by neutrons being scattered from the sample. While the detection setup itself has been optimized for low sensitivity to these scattered neutrons, some residual background may be induced due to capture events in any other material present in the experimental area. For resonance fitting, this background was taken into account by assuming a constant background below the resonance. For the unresolved resonance region, the background was

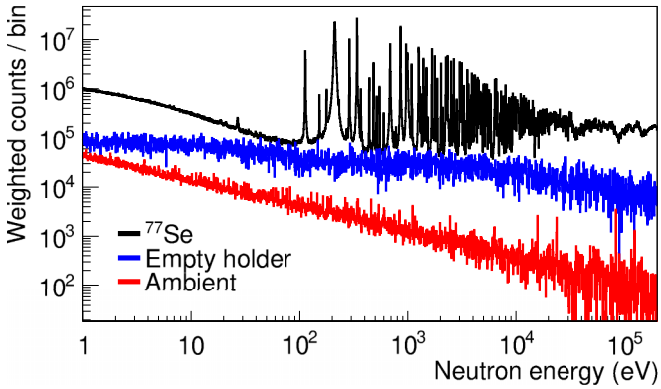

FIG. 1. Weighted counts as a function of neutron energy for the ^{77}Se sample (black), empty sample holder (blue), and ambient experimental area background (red).

determined using a natural carbon sample (see Table I), as the carbon neutron scattering cross section is ≈2000 times higher than capture in the neutron energy region of interest. The spectra measured with the carbon sample were scaled for areal density and scattering cross sections and then subtracted from the ^{77}Se spectrum. The level of this background relative to ^{77}Se was at most 1.5% in the relevant neutron energy region. Assuming 20% uncertainty in the background determination, dominated by the uncertainty of the ^{77}Se scattering cross section, the uncertainty on the capture yield due to the background subtraction is 0.3%.

3. Neutron fluence and normalization

The energy dependence of the neutron flux at n_TOF EAR-1 was measured using the reference reactions ^{10}B(n,α) and ^{235}U(n,f) in a separate campaign [20], with uncertainties ranging from 1% to 5% in the energy range of interest. In addition, the neutron fluence is continuously monitored with a set of off-beam silicon detectors using ^{6}Li(n,t) reactions on a thin ^{6}LiF sample deposited on a Mylar backing. An absolute normalization factor $f(E_n)$ is required to account for the fact that the neutron beam size (which slightly varies with neutron energy) is larger than the sample, and to correct for any inaccuracies in the solid angle coverage of the detectors used in the GEANT4 simulations. Selenium yields were normalized to the 4.9 eV resonance in the ^{197}Au(n,γ) reaction, using the saturated resonance technique [21]. The thickness of the gold sample was chosen so that all neutrons incident on the Au target are captured and produce a γ-ray cascade, allowing determination of $f(E_n)$ at $E_n = 4.9$ eV with high accuracy. The energy dependence of normalization caused by the energy dependence of the neutron beam size was determined in detailed simulations of the neutron transport from the spallation target to the experimental area and verified experimentally [14]. Corrections never exceeded 2%. The uncertainty of the $f(E_n)$ is 1%.

B. Parameters of isolated resonances

Neutron resonances in the capture yield determined in equation (1) were analysed using the multilevel multi-channel R-matrix code SAMMY [22]. SAMMY fits resonance parameters, i.e., resonance energy E_R and neutron and radiative widths for a given resonance spin J and parity π. Experimental effects, such as resonance broadening due to thermal motion of atoms (Doppler broadening) and the resolution of the experimental facility, as well as multiple interaction and self shielding of neutrons in the sample material, are taken into account. In general, capture data alone do not allow one to reliably determine all resonance parameters, Γ_γ, Γ_n, E_R, J, and π. Thus the table in the Supplemental Material [23] provides only resonance energy E_R and capture kernel K, defined as

$$K = g\frac{\Gamma_\gamma \Gamma_n}{\Gamma_\gamma + \Gamma_n}, \tag{2}$$

with

$$g = \frac{2J+1}{(2I+1)(2s+1)}, \tag{3}$$

where I is the spin of the ground state of the target nucleus ($I^\pi = \frac{1}{2}^-$ for ^{77}Se), and $s = \frac{1}{2}$ is the neutron spin. Values for all identified resonance structures up to 51 keV are tabulated in the Supplemental Material [23]. The uncertainties listed in the table are only those coming from the fit. Systematic uncertainties comprise 3% from PHWT, 1% from normalization, 1% to 5% from flux, and 0.01% in sample composition and mass. The total systematic uncertainty is thus 3.3% below neutron energy of 100 eV, 3.7% between 100 eV and 10 keV, and 5.9% above 10 keV. Figure 2 then compares the SAMMY fit to the data for several energy regions.

The resonance spins, considered in SAMMY fitting, are known only for a very restricted set of resonances. For resonances listed in the ENDF/B-VIII.0 database [12], we used the spin assignment from this database for the majority of them. Three s-wave resonances at 483, 1780, and 2033 eV [6,7] had their spins reassigned based on analysis of the γ-ray energy spectra deposited in C_6D_6 detector.

Following s-wave neutron capture on ^{77}Se, a resonance with $J^\pi = 0^-$ or 1^- can be formed, while ^{78}Se has predominantly only 0^+ and 2^+ states below an excitation energy of ≈3 MeV. Direct γ-ray transitions from $J = 0^-$ resonances to these states are then expected to be very weak, while the transitions from $J = 1^-$ can be significantly stronger. Therefore, the spectral shape is expected to be different for the different resonance spins for deposited energy $E_D \gtrsim 8$ MeV (the neutron separation energy of ^{77}Se is $S_n = 10.498$ MeV [24]). Figure 3 illustrates this feature. Panel (a) shows the noticeable excess of intensity for high E_D from 1^- resonances with respect to 0^- resonance (note that counts for $E_D > S_n$ are observed due to the C_6D_6 detector's poor energy resolution). To increase statistics a sum of three strong 1^- resonances is shown. The energy spectra are normalized in the total number of counts. Spins of all the 1^- resonances were assigned by Coté *et al.* [6], while the spin of the 211-eV 0^- resonance was assigned by Refs. [6–8].

Panel (b) then gives a fraction of counts for $E_D = 8$–10.5 MeV to the total number of counts for s-wave resonances with sufficient statistics. Resonances with the highest fraction definitely have $J = 1$. This should be the case

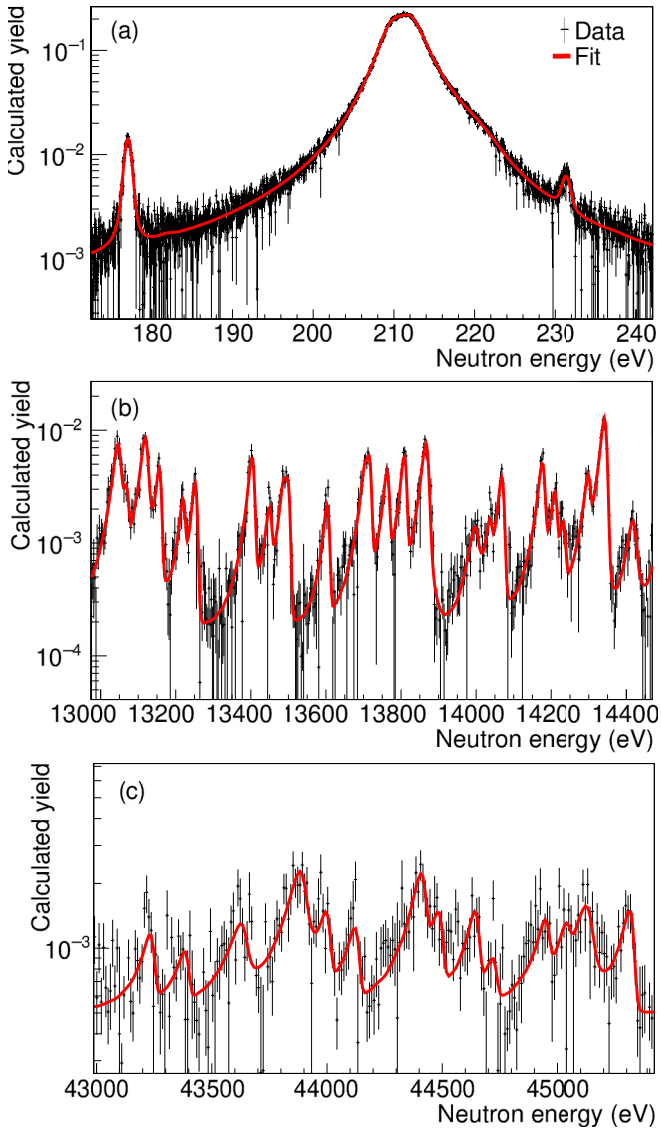

FIG. 2. Examples of SAMMY fits (red) to ^{77}Se(n,γ) yield data (black).

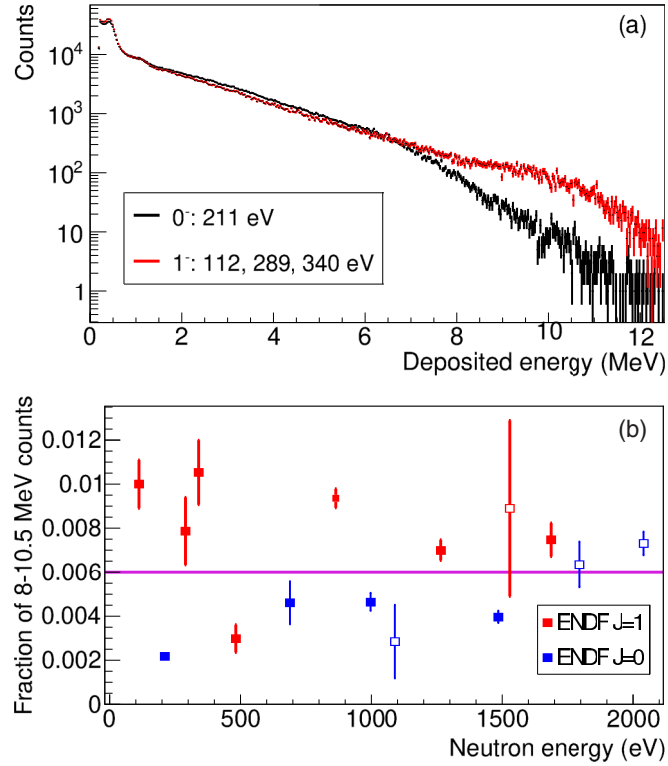

FIG. 3. (a) Deposited energy spectra for one 0^- resonance and a sum of three 1^- resonances. (b) Fraction of counts for deposited energy E_D = 8–10.5 MeV to the total number of counts for resonances with sufficient statistics. The line indicates the adopted threshold to differentiate between the two spin assignments ($J^\pi = 0^-$ and 1^- below and above the line, respectively) used in resonance fits with SAMMY. Empty squares indicate resonances where no measured spin data are available in Refs. [6–8].

of all resonances above the indicated line. For all resonance below the line we then considered $J = 0$, although those with the ratio close to the line could still have $J^\pi = 1^-$. Using this criterion, the 483-eV resonance had spin reassigned from the ENDF value of 1^- to 0^-, and resonances at 1780 and 2033 eV from 0^- to 1^-. It should be noted that from these three cases, only the 483 eV resonance had its spin in ENDF assigned based on experimental data [6], while the other two had spins assigned based on the random number method [12]. In practice, it shows that values of K obtained under different assumptions on resonance spin are fully consistent within uncertainties. This feature allows determination of the cross section using the kernel K without firm knowledge of the resonance J^π.

C. Unresolved resonance region

Although resonance kernels for individual resonance structures were determined for neutron energies up to 51 keV, from about 20 keV onward we expect that a non-negligible fraction of resonances is either not completely resolved or missed due to a combination of worsening of neutron energy resolution and lower counting statistics. Missing resonances would then lead to an underestimation of MACS deduced from listed capture kernels K. Therefore, we extracted the unresolved resonance region (URR) cross section in the energy region of 20–200 keV. Using simulations based on a statistical model (see below), we estimate that missing resonances below 20 keV account at most for ≈1.5% of the MACS for any kT; this fraction is much smaller than the obtained uncertainty of MACS.

Data in the URR region had neutron scattering background subtracted based on carbon sample data (see Sec. III A 2), and the experimental yield was corrected for multiple neutron interactions and self-shielding. The latter corrections were estimated using a Monte Carlo code which takes into account the sample properties, as well as neutron capture and scattering cross sections from the JEFF 3.3 library [25]. The same approach has been used in the analysis of n_TOF data from a number of previous experiments; see Ref. [26] and references therein. Corrections to the measured yield were around 3% in the relevant energy range. Besides the systematic uncertainties considered for resolved resonances, the contributions

TABLE II. Cross sections for several average neutron energies measured by Kamada *et al.* [3] compared to averaged cross sections obtained in this work. The listed uncertainties represent the statistical and systematic contributions.

Kamada *et al.*		n_TOF	
Average energy (range) (keV)	Cross section (mb)	Energy interval (keV)	Cross section (mb)
21 (15–25)	619 ± 24	17–25	663 ± 40
30 (25–35)	514 ± 20	25–35	558 ± 34
45 (35–55)	420 ± 16	35–55	453 ± 27
70 (55–100)	326 ± 12	55–85	350 ± 21

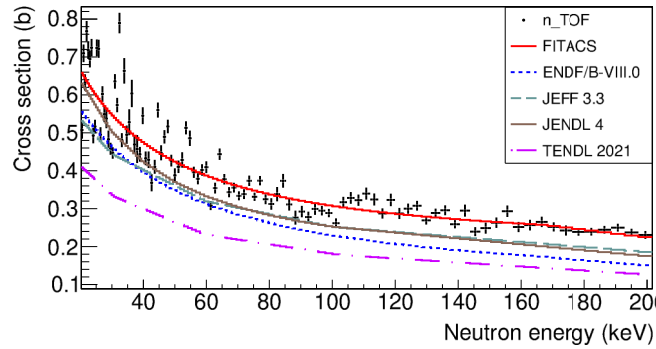

FIG. 4. A comparison of the ^{77}Se(n,γ) URR cross section obtained in this work with evaluations [12,25,27,28] and FITACS [29] fit to our data.

due to scattered neutrons (0.3%) and multiple-interaction and self-shielding correction (0.5%) affect the total systematic uncertainty in the URR cross section. The flux uncertainty is 5% up to 100 keV neutron energy and 2% in the 100–200 keV energy region. The total systematic uncertainty in URR is thus 5.9% below 100 keV and 3.8% above that energy.

We can compare our URR cross section to the only other available measurement by Kamada *et al.* [3,4], who provide spectrum averaged cross sections in four energy intervals from 15 to 100 keV. Table II shows a comparison of their results (obtained from neutron spectra shown in Fig. 2 of Ref. [3]) to our cross sections, which have been averaged over an energy interval that results in the same average neutron energy as data by Kamada *et al.* Our averaged cross sections are consistently 7–8% higher, but still in agreement with Kamada *et al.* within uncertainties.

Figure 4 shows our cross section in the URR compared to recent evaluations ENDF/B-VIII.0 [12], JEFF 3.3 [25], JENDL-4 [27], and TENDL 2021 [28]. Up to 100 keV neutron energy, ENDF, JEFF, and JENDL evaluations underestimate our cross section by about 10–15% on average and TENDL by almost 40%, while for 100–200 keV neutron energies JEFF and JENDL underestimate the cross section by ≈20%, ENDF by ≈30%, and TENDL by ≈40%.

D. Average resonance parameters

Using the individual resonance parameters obtained from SAMMY fitting, some of the average resonance parameters can be constrained. For instance, for resonances with $\Gamma_n \gg \Gamma_\gamma$, $g\Gamma_\gamma$ and Γ_n can be reasonably determined. Values of Γ_n allow in some cases identification of s-wave character of the resonance. For the determination of average resonance parameters, we assumed that there are no unresolved doublets or even more complex structures below 17 keV.

Due to the limitations in the time-of-flight method in unambiguously assigning spins, we cannot easily obtain Γ_γ for a significant fraction of resonances. However, for the strongest resonances in Γ_n (with $\Gamma_n \gg \Gamma_\gamma$ and $K \approx g\Gamma_\gamma$) that are definitely of the s-wave character we can adopt the following approach. If we assume that the Γ_γ distribution is independent of resonance spin and parity then we can write $\langle g\Gamma_\gamma \rangle = \langle g \rangle \times \langle \Gamma_\gamma \rangle$. An estimate of $\langle g \rangle$ can be obtained if the spin distribution of considered resonances is known. We estimated $\langle g \rangle$ for these resonances using simulations based on the statistical model, i.e., assuming Porter-Thomas distribution of reduced neutron widths, normal distribution of Γ_γ, and Wigner spacing of neighboring resonances with the same J^π. Furthermore, the spin dependence from Ref. [30] was assumed along with parity independence of the resonance density.

Considering 43 resonances below 17 keV with SAMMY fits resulting in $\Gamma_n > 15K$, we obtain $\langle \Gamma_\gamma^{\ell=0} \rangle \approx 410(50)$ meV (including 7% uncertainty in $\langle g \rangle$ coming from the statistical model), which is in a good agreement with $\langle \Gamma_\gamma^{\ell=0} \rangle = 390(54)$ meV provided by Mughabghab [11]. It is to be noted that the $\langle \Gamma_\gamma \rangle$, as well as Γ_γ distribution width σ_{Γ_γ}, might not be identical for all resonance spins and parities. Specifically, simulations based on the statistical model of the nucleus with the DICEBOX [19] code indicate that $\langle \Gamma_\gamma \rangle$ from 1^- resonances can be expected to be larger by about 10–20% than for the other s- and p-wave resonances.

The strongest resonances in terms of Γ_n can be also used for determination of the s-wave neutron strength function S_0. From the neutron energy region below 17 keV we obtained $S_0 = 1.5(2) \times 10^{-4}$, in agreement with $S_0 = 1.49(38) \times 10^{-4}$ available in Ref. [11]. The analysis of the sum of Γ_n in various regions also indicated that $S_1 = 2.4(6) \times 10^{-4}$ considering channel radius $R = 1.35A^{1/3}$ fm $= 6.03$ fm.

For determination of D_0, a method similar to that used in the analyses of previous n_TOF measurements [26,31,32] was adopted. We compared the observed number of resonances with a kernel higher than a threshold with predictions from aforementioned simulations based on the statistical model. Several different thresholds and maximum neutron energies were adopted in testing. All their combinations yielded results consistent with $D_0 = 110(15)$ eV. The deduced D_0 was found to be largely independent of exact values of S_ℓ and parameters of Γ_γ distributions if their values were consistent with those mentioned above. Our D_0 value is in agreement with 110(11) eV reported in Ref. [11].

We also used URR cross section data in the range $E_n = 20$–200 keV to estimate average resonance parameters using the FITACS package in SAMMY [22,29]. Fixing D_0 to 110 eV and setting channel radius to $R = 6.03$ fm

yielded $S_0 = 1.38(34) \times 10^{-4}$, $S_1 = 2.31(28) \times 10^{-4}$, $S_2 = 2.58(41) \times 10^{-4}$, $\Gamma_\gamma^{\ell=0} = \Gamma_\gamma^{\ell=2} = 369(37)$ meV, and $\Gamma_\gamma^{\ell=1} = 380(18)$ meV. The S_0, S_1, and $\Gamma_\gamma^{\ell=0}$ are in a good agreement with the values deduced from resolved resonances. We note that $S_1 = 4.3(10) \times 10^{-4}$ in Ref. [11] is significantly larger than the value found in our analysis.

IV. STELLAR CROSS SECTIONS AND ASTROPHYSICAL IMPLICATIONS

The Maxwellian averaged cross section (MACS) is defined as

$$\text{MACS} = \frac{2}{\sqrt{\pi}} \frac{1}{(kT)^2} \int_0^\infty E\sigma(E) \exp\left(-\frac{E}{kT}\right) dE. \quad (4)$$

We calculated MACSs for kT values from 5 to 100 keV, covering stellar temperatures of roughly 0.06–1.2 GK by combining three neutron energy regions: (i) below 20 keV we used the resonance parameters determined in SAMMY, (ii) from 20 to 200 keV we used the URR cross section derived from our data, and (iii) above 200 keV we used cross section from JEFF 3.3 scaled by a factor of 1.18, corresponding to the previously-mentioned difference between JEFF 3.3 and n_TOF cross sections in the 100–200 keV range. 20% uncertainty was assumed for the latter region.

Due to the high temperatures in stellar environments, nuclei may not only be present in their ground state, but also in thermally excited states. This means that the effective stellar MACS* does not correspond to the ground state one determined in a laboratory experiment, but needs to be corrected to take into account neutron capture on the excited states. In the case of ^{77}Se, nearly 100% of nuclei are expected to be in their ground state for stellar temperatures around 0.1 GK, while this number reduces to ≈38% at 1 GK. TALYS 1.9 [33] was used to calculate theoretical ground state MACS and stellar MACS* values. For this calculation, we renormalized average level spacing and radiative widths to those obtained from resolved resonance data analysis, while leaving all other parameters in their default settings. For the ground state MACS we obtained values lower than the experimental data with a difference of about 15% for all values of kT.

TALYS calculations using the JLM (Jeukenne, Lejeune, and Mahaux) optical model potential [34] then resulted in MACS values lower by 10–25% than the default potential depending on kT. Thus, in order to estimate the contribution of nuclei in excited states to MACS*, we adopted the results from calculations with the default optical model potential with 25% uncertainty. We then employ the procedure described in Refs. [35,36], by combining our experimental ground-state MACS with excited state contributions calculated using TALYS, to determine updated MACS* and its uncertainties. While experimental ground state MACS exhibit uncertainties from 4.2% at $kT = 5$ keV to 5.7% at $kT = 100$ keV, MACS* uncertainties range from 4.2% at $kT = 5$ keV to 18% at $kT = 100$ keV.

Table III lists n_TOF MACS and MACS* for kT between 5 and 100 keV and MACS from the KADoNiS v0.3 database [37]. The latter come from calculations by Bao *et al.* [38] and are 24–32% lower across the entire temperature range compared to the n_TOF MACS.

TABLE III. Maxwellian-averaged cross section values calculated for the ^{77}Se(n,γ) reaction based on n_TOF experimental data compared to values available in KADoNiS v0.3 for energies kT between 5 and 100 keV. MACS values consider only ground-state contribution, while MACS* also includes excited state contributions at given kT.

kT (keV)	n_TOF MACS (mb)	n_TOF MACS* (mb)	KADoNiS v0.3 MACS (mb)
5	1485 ± 63	1485 ± 63	999
10	995 ± 48	995 ± 48	695
15	794 ± 41	794 ± 41	582
20	680 ± 36	680 ± 36	510
25	605 ± 33	604 ± 34	458
30	550 ± 30	548 ± 33	418 ± 71
40	475 ± 25	467 ± 35	360
50	423 ± 21	406 ± 39	319
60	384 ± 19	357 ± 42	287
80	326 ± 17	283 ± 44	240
100	283 ± 16	233 ± 42	205

The experimentally determined MACS can be also used for constraining models used in reaction codes for cross section calculation. TENDL 2021 library [28] provides predictions of MACS for $kT = 30$ keV obtained with different models used in the TALYS 1.96 reaction code [33]. These predictions cover a broad range of values from 200 to 700 mb. TENDL also offers a set of 12 preferred models with calculated MACS range of 295–527 mb. Our experimental value agrees within the uncertainty only with two of these 12 models.[1]

We quantified the impact of our new MACS* for a $15M_\odot$ star with a subsolar metallicity of $Z = 0.006$. The stellar structure was computed in Ref. [40], and the choice of this specific metallicity was motivated by the peak in weak s-process elements production that occurs at $Z = 0.006$ (details in Ref. [40]). We calculated the full nucleosynthesis in a postprocessing step using the multizone nucleosynthesis code MPPNP [41]. Compared to using the default ^{77}Se(n,γ) MACSs (KADoNiS v0.3), the MACS* values obtained in this study lead to a reduction of 14% of ^{77}Se abundances, while other isotopic abundances are only negligibly affected.

A further investigation of effects induced by our MACS* on the s-process nucleosynthesis has been conducted with stellar models of low-mass AGB stars computed with the FUNS code [42–44]. Two models, with metallicities representative of the galactic halo ($Z = 0.002$) and disk ($Z = 0.02$), and mass equal to $2M_\odot$ were considered. The adoption of the new MACS* results in a 19% and 14% lower ^{77}Se production, respectively. No other meaningful variations are found for the $Z = 0.002$ model, while only modest increases ($\leqslant 5\%$) in the

[1]Experimental MACS agreement was found for models 9 and 10 in TENDL 2021. TENDL results and model descriptions are available at [39].

abundance of other heavy isotopes occurs for the Z = 0.02 one, with respect to the models computed using the KADoNiS v0.3 ^{77}Se MACS.

V. SUMMARY

The ^{77}Se(n,γ) cross section was measured up to 200 keV neutron energy at the n_TOF facility at CERN. Resonance energies and capture kernels for neutron energies up to 51 keV were determined using the *R*-matrix code SAMMY, and the unresolved cross section was determined up to 200 keV neutron energy. All resonances above 4 keV are reported for the first time, and we have identified new resonances also below 4 keV. Obtained individual resonance parameters allowed constraining of average resonance parameters. These parameters were fully consistent with those obtained using FITACS code from the unresolved resonance region and (with the exception of S_1) also with values available in Ref. [11]. Our unresolved cross section between 15 and 100 keV is about 7–8% higher than the only available measurement by Kamada *et al.* [3].

Maxwellian averaged cross sections were calculated for kT between 5 and 100 keV. They are up to 32% higher than the values recommended in the KADoNiS v0.3 database for all stellar temperatures. We have investigated the impact of our new cross section results on *s*-process nucleosynthesis in a massive star and found a 14% decrease of ^{77}Se abundances for a $15M_\odot$, $Z = 0.006$ star compared to using KADoNiS v0.3 MACS values. Similarly, 19% and 14% decreases were found in ^{77}Se abundance in $Z = 0.002$ and $Z = 0.02$ stars of mass $2M_\odot$, respectively.

ACKNOWLEDGMENTS

This work was supported by the UK Science and Facilities Council (ST/M006085/1), the MSMT of the Czech Republic, the Charles University UNCE/SCI/013 project, the European Research Council ERC-2015-StG No. 677497, and by the funding agencies of the participating institutes. In line with the principles that apply to scientific publishing and the CERN policy in matters of scientific publications, the n_TOF Collaboration recognizes the work of Y. Kopatch and V. Furman (JINR, Russia), who have contributed to the experiment used to obtain the results described in this paper.

[1] C. M. Raiteri, R. Gallino, M. Busso, D. Neuberger, and F. Käppeler, Astrophys. J. **419**, 207 (1993).
[2] N. Nishimura, R. Hirschi, T. Rauscher, A. St. J. Murphy, and C. Cescutti, Mon. Not. R. Astron. Soc. **469**, 1752 (2017).
[3] S. Kamada, M. Igashira, T. Katabuchi, and M. Mizumoto, J. Nucl. Sci. Technol. **47**, 634 (2010).
[4] M. Igashira, S. Kamada, T. Katabuchi, and M. Mizumoto, J. Korean Phys. Soc. **59**, 1665 (2011).
[5] J. M. LeBlanc, R. E. Coté, and L. M. Bollinger, Nucl. Phys. **14**, 120 (1959).
[6] R. E. Coté, L. M. Bollinger, and G. E. Thomas, Phys. Rev. **136**, B703 (1964).
[7] Kh. Maletski, L. B. Pikel'ner, I. M. Salamatin, and E. I. Sharapov, Sov. J. Nucl. Phys. **9**, 1119 (1969).
[8] J. Julien, R. Alves, S. de Barros, V. D. Nuynh, J. Morgenstern, and C. Samour, Nucl. Phys. A **132**, 129 (1969).
[9] J. Hori, H. Yashima, S. Nakamura, K. Furutaka, K. Y. Hara, H. Harada, K. Hirose, A. Kimura, F. Kitatani, M. Koizumi, M. Oshima, Y. Toh, M. Igashira, T. Katabuchi, M. Mizumoto, T. Kamiyama, K. Kino, and Y. Kiyanagi, Nucl. Data Sheets **119**, 128 (2014).
[10] X.-R. Hu, L.-X. Liu, W. Jiang, J. Ren, G.-T. Fan, H.-W. Wang, X.-G. Cao, L.-L. Song, Y.-D. Liu, Y. Zhang, X.-X. Li, Z.-R. Hao, P. Kuang, X.-H. Wang, J.-F. Hu, B. Jiang, D.-X. Wang, S. Zhang, Zh.-D. An, Y.-T. Wang *et al.*, Chin. Phys. B **31**, 080101 (2022).
[11] S. F. Mughabghab, *Atlas of Neutron Resonances*, 6th ed. (Elsevier, Amsterdam, 2018), pp. 386–387.
[12] D. A. Brown, M. B. Chadwick, R. Capote, A. C. Kahler, A. Trkov, M. W. Herman, A. A. Sonzogni, Y. Danon, A. D. Carlson, M. Dunn, D. L. Smith, G. M. Hale, G. Arbanas, R. Arcilla, C.R. Bates, B. Beck, B. Becker, F. Brown, R. J. Casperson, J. Conlin *et al.*, Nucl. Data Sheets **148**, 1 (2018).
[13] The n_TOF Collaboration, n_TOF - The Neutron Time-of-Flight Facility at CERN, http://www.cern.ch/ntof (2022).
[14] C. Guerrero *et al.* (n_TOF collaboration), Eur. Phys. J. A **49**, 1 (2013).
[15] P. F. Mastinu, R. Baccomi, E. Berthoumieux, D. Cano-Ott, F. Gramegna, C. Guerrero, C. Massimi, P. M. Milazzo, F. Mingrone, J. Praena, G. Prete, and A. R. García, New C_6D_6 detectors: Reduced neutron sensitivity and improved safety, CERN Report No. n_TOF-PUB-2013-002, 2013 (unpublished).
[16] P. Žugec *et al.* (n_TOF collaboration), Nucl. Instrum. Methods Phys. Res., Sect. A **812**, 134 (2016).
[17] U. Abbondanno *et al.* (n_TOF collaboration), Nucl. Instrum. Methods Phys. Res., Sect. A **521**, 454 (2004).
[18] S. Agostinelli *et al.* (GEANT4 Collaboration), Nucl. Instrum. Methods Phys. Res., Sect. A **506**, 250 (2003).
[19] F. Bečvář, Nucl. Instrum. Methods Phys. Res., Sect. A **417**, 434 (1998).
[20] M. Barbagallo *et al.* (n_TOF collaboration), Eur. Phys. J. A **49**, 156 (2013).
[21] R. L. Macklin, J. Halperin, and R. R. Winters, Nucl. Instrum. Methods **164**, 213 (1979).
[22] N. M. Larson, Updated users guide for SAMMY: Multilevel R-matrix fits to neutron data using Bayes' equations, Oak Ridge National Laboratory Technical Report No. ORNL/TM-9179/R8, 2008 (unpublished).
[23] See Supplemental Material at http://link.aps.org/supplemental/10.1103/PhysRevC.107.065805 for a list of measured ^{77}Se resonance energies and kernels.
[24] A. R. Farhan and B. Singh, Nucl. Data Sheets **110**, 1917 (2009).
[25] A. J. M. Plompen, O. Cabellos, C. De Saint Jean, M. Fleming, A. Algora, M. Angelone, P. Archier, E. Bauge, O. Bersillon, A. Blokhin, F. Cantargi, A. Chebboubi, C. Diez, H. Duarte, E. Dupont, J. Dyrda, B. Erasmus, L. Fiorito, U. Fischer, D. Flammini *et al.*, Eur. Phys. J. A **56**, 181 (2020).

[26] M. Dietz *et al.* (n_TOF Collaboration), Phys. Rev. C **103**, 045809 (2021).
[27] K. Shibata, O. Iwamoto, T. Nakagawa, N. Iwamoto, A. Ichihara, S. Kuneida, S. Chiba, K. Furutaka, N. Otuka, T. Ohsawa, T. Murata, H. Matsunobu, A. Zukeran, S. Kamada, and J. Katakura, J. Nucl. Sci. Technol. **48**, 1 (2011).
[28] A. J. Koning, D. Rochman, J.-Ch. Sublet, N. Dzysiuk, M. Fleming, and S. van der Marck, Nucl. Data Sheets **155**, 1 (2019).
[29] F. Fröhner, B. Goel, and U. Fischer, FITACS, Argonne National Laboratory Technical Report No. ANL-83-4, 1983 (unpublished).
[30] T. von Egidy and D. Bucurescu, Phys. Rev. C **72**, 044311 (2005).
[31] J. Lerendegui-Marco *et al.* (n_TOF Collaboration), Phys. Rev. C **97**, 024605 (2018).
[32] A. Gawlik *et al.* (n_TOF collaboration), Phys. Rev. C **100**, 045804 (2019).
[33] A.J. Koning, TALYS-1.9, https://www.talys.eu (2021).
[34] E. Bauge, J. P. Delaroche, and M. Girod, Phys. Rev. C **63**, 024607 (2001).
[35] T. Rauscher, Astrophys. J. Lett. **755**, L10 (2012).
[36] T. Rauscher, Astrophys. J. **864**, 40 (2018).
[37] The Karlsruhe Astrophysical Database of Nucleosynthesis in Stars 1.0 (test version), online at https://www.kadonis.org/, latest release Kadonis-0.3; I. Dillmann, M. Heil, F. Käppeler, R. Plag, T. Rauscher, and F. K. Thielemann, Am. Inst. Phys. Conf. Ser. **819**, 123 (2006).
[38] Z.Y. Bao, H. Beer, F. Käppeler, F. Voss, and K. Wisshak, At. Data Nucl. Data Tables **76**, 70 (2000).
[39] https://tendl.web.psi.ch/tendl_2021/tar_files/astro/12.models/macs/audi/Se/Se077.txt.
[40] C. Ritter, F. Herwig, S. Jones, M. Pignatari, C. Fryer, and R. Hirschi, Mon. Not. R. Astron. Soc. **480**, 538 (2018).
[41] F. Herwig, M. E. Bennett, S. Diehl, C. L. Fryer, R. Hirschi, A. Hungerford, G. Magkotsios, M. Pignatari, G. Rockefeller, F. X. Timmes, and P. Young, in *Proceedings of 10th Symposium on Nuclei in the Cosmos*, PoS NIC X (Sissa Medialab srl Via Bonomea, Trieste, Italy, 2009), p. 023.
[42] S. Cristallo, L. Piersanti, O. Straniero, R. Gallino, I. Domínguez, C. Abia, G. Di Rico, M. Quintini, and S. Bisterzo, Astrophys. J. Suppl. Ser. **197**, 17 (2011).
[43] D. Vescovi, S. Cristallo, M. Busso, and N. Liu, Astrophys. J. Lett. **897**, L25 (2020).
[44] D. Vescovi, S. Cristallo, S. Palmerini, C. Abia, and M. Busso, Astron. Astrophys. **652**, A100 (2021).